

# Completing density functional theory by machine-learning hidden messages from molecules

Ryo Nagai<sup>1,2,\*</sup>, Ryosuke Akashi<sup>1</sup>, and Osamu Sugino<sup>1,2</sup>

<sup>1</sup>*Department of Physics, The University of Tokyo, Hongo, Bunkyo-ku, Tokyo 113-0033, Japan and*

<sup>2</sup>*Institute for Solid State Physics, The University of Tokyo, Kashiwa, Chiba 277-8581, Japan*

(Dated: March 7, 2019)

Kohn-Sham(KS) density functional theory<sup>1,2</sup>(DFT) is the base of modern computational approaches to electronic structures. Their accuracy vitally relies on the exchange-correlation energy functional, where all the electron-electron interaction beyond the classical Coulomb one are encapsulated. Improving the functional has long been the major topic of DFT but the past approaches remain heuristic rather than systematic. Here we demonstrate a systematic way to machine-learn the functional from accurate density and energy calculated for a few molecules. After relating the density and energy with a flexible feed-forward neural network, the network is optimized to reproduce the accurate ones within KS-DFT, of which the exchange-correlation potential is obtained by taking functional derivatives with a help of the back-propagation method<sup>3</sup>. The machine-learned functionals show comparable or improved accuracies to the existing ones. In addition, one can naturally extend the scheme to a non-local one by simply adding the nodes connected to the hidden layers, thus allowing to construct various functionals of different accuracy and complexity. This novel approach thus paves a way to enriching the DFT framework by utilizing the rapidly advancing machine learning techniques.

In KS-DFT, solution of the KS equation

$$\left[ -\frac{\nabla^2}{2} + V_{\text{ion}}(\mathbf{r}) + \int d\mathbf{r}' \frac{n(\mathbf{r}')}{|\mathbf{r}-\mathbf{r}'|} + V_{\text{xc}}(\mathbf{r}) \right] \varphi_i(\mathbf{r}) = \varepsilon_i \varphi_i(\mathbf{r}), \quad (1)$$

with the density  $n(\mathbf{r})$  calculated by summing  $|\varphi_i(\mathbf{r})|^2$  for all the occupied states, yields the total energy as well as electron density distribution of an interacting electron system under the ionic potential  $V_{\text{ion}}$ . The exchange-correlation (xc) potential  $V_{\text{xc}}$  is ideally a non-local functional of the whole distribution of the density, where its value at  $\mathbf{r}$  is affected by  $\{n(\mathbf{r})\}$ , but its explicit form has yet been elusive. Enormous effort has been devoted to heuristically develop the functional either in a purely local form, where  $V_{\text{xc}}(\mathbf{r})$  depends only on  $n(\mathbf{r})$ , in a form semi-locally corrected using gradient  $\nabla n(\mathbf{r})$ , or in a form non-locally corrected with  $\{\varphi_i\}$ , thereby gradually climbing the so-called Jacob's ladder<sup>4</sup> of accuracy in exchange for complexity and cost-up. However, in order to determine the formulas including those components, one generally has to exploit elaborate combinations of the perturbation theory, analyses of asymptotic behaviors

of physical quantities, and fitting to references such as numerically expensive calculations and experimental observations. Medvedev and coworkers have warned that some modern functionals thus formulated could yield less-accurate density distribution than those from previous ones<sup>5</sup>.

The pivotal problem is that, unlike the perturbation theory for the physical quantities<sup>6</sup>, the formula of  $V_{\text{xc}}$  cannot be directly derived since it is defined implicitly—the function that reproduce the exact  $n(\mathbf{r})$  through Eq. 1 for any systems. Alternatively, a machine-learning approach have been proposed to construct an explicit form of  $V_{\text{xc}}$ <sup>7</sup>. There, the neural network as the mapping  $n \rightarrow V_{\text{xc}}$  is trained with accurate reference pair(s) of the  $[n, V_{\text{xc}}]$  prepared by solving numerically interacting Hamiltonian. The NN potential thus trained has been demonstrated to be applicable also to other systems (transferable) for a low dimensional model case. Along this line, we explore a widely transferable NN-based density functional for realistic systems.

Precisely, we assume the following form for the xc-energy  $E_{\text{xc}}[n]$  to obtain the xc-potential by  $V_{\text{xc}}(\mathbf{r}) = \delta E_{\text{xc}} / \delta n(\mathbf{r})$ :

$$E_{\text{xc}}[n] \equiv \int d\mathbf{r} n(\mathbf{r}) \varepsilon_{\text{xc}}(\mathbf{g}[n](\mathbf{r})) \quad (2)$$

where  $\mathbf{g}[n](\mathbf{r})$  represents any variables depending on density distribution around  $\mathbf{r}$ . Most of existing functionals adopt local spin density approximation(LSDA)<sup>8,9</sup>, generalized gradient approximation(GGA)<sup>10-12</sup>, or meta-GGA<sup>13-15</sup>, by defining  $\mathbf{g}[n](\mathbf{r})$  as  $(n(\mathbf{r}), \zeta(\mathbf{r}))$  or  $(n_{\uparrow}(\mathbf{r}) - n_{\downarrow}(\mathbf{r})) / n(\mathbf{r}), (n(\mathbf{r}), \zeta(\mathbf{r}), s(\mathbf{r})) \equiv (|\nabla n(\mathbf{r})| / n^{4/3}(\mathbf{r}))$ , or  $(n(\mathbf{r}), \zeta(\mathbf{r}), s(\mathbf{r}), \tau(\mathbf{r})) \equiv 1/2 \sum_i^{\text{occ}} |\nabla \phi_i(\mathbf{r})|^2$  respectively. In this study, the xc-energy density  $\varepsilon_{\text{xc}}$  is formulated with the feed-forward NN with  $H$  layers, which is a vector-to-vector mapping  $\mathbf{u} \rightarrow \mathbf{v}$  represented by

$$\mathbf{v} = h_H(\dots(h_2(h_1(\mathbf{u}))) \quad (3)$$

$$h_i(\mathbf{x}) \equiv f(\mathbf{x}W_i + \mathbf{b}_i). \quad (4)$$

The  $h_i$  represent the  $i$ -th layer of NN, where the input vector  $\mathbf{x}$  is non-linearly transformed by the activation function  $f$  after the linear transformation by the weight parameters  $W_i$  and  $\mathbf{b}_i$ . The biggest advantage of using NN is that this form can represent any well-behaved functions with arbitrary numerical error by increasing the number of nodes<sup>16</sup> (the dimension of the matrices  $W_1, \dots, W_H$ ). Here we define  $\mathbf{u}$  as the local values  $\mathbf{g}[n](\mathbf{r})$  and  $\mathbf{v}$  as one-dimensional vector  $\varepsilon_{\text{xc}}(\mathbf{r})$  (see Method for

the exact definition). In the functional derivative of  $E_{xc}/n(\mathbf{r})$  to obtain  $V_{xc}(\mathbf{r})$ , we can utilize the backpropagation method<sup>3</sup>, which is an efficient algorithm to calculate the chain rules in a NN. This NN form therefore relates  $\{n(\mathbf{r})\}$  and  $\{V_{xc}(\mathbf{r})\}$ , and is incorporated in the KS equation.

We prepared four cases for the input vector  $\mathbf{g}$ ; LSDA, GGA, meta-GGA and also a new formulation we call "near region approximation" (NRA)  $\mathbf{g}[n](\mathbf{r}) = (n(\mathbf{r}), \zeta(\mathbf{r}), s(\mathbf{r}), \tau(\mathbf{r}), R(\mathbf{r}))$ , where  $R(\mathbf{r}) \equiv \int d\mathbf{r}' n(\mathbf{r}') \exp(-|\mathbf{r} - \mathbf{r}'|/\sigma)$ . Gunnarsson et al.<sup>17</sup> showed that such an averaged density around  $\mathbf{r}$  describes  $\varepsilon_{xc}(\mathbf{r})$  efficiently, therefore we combine it into the  $\mathbf{g}$  of meta-GGA. It is emphasized that theoretical determination of a functional including such a non-locality is impractically complex without using a systematic machine-learning approach.

To train the NN, we need as many accurate training dataset as the NN parameters, which are obtained from numerically expensive calculations or experimental observations. In some construction of existing functionals, scalar quantities such as energies of many systems are referred of many systems of the parameters. We, on the other hand, take the whole electron density distribution of a few systems as the target. The requirement of reproducing  $\{n(\mathbf{r})\}$  over the three-dimensional space through solving the KS equation makes this task a (over-)determined problem with a sufficient number of numerical grid points. Also, unlike the major application of the machine-learning scheme to electronic structures, which avoids solving the KS equation<sup>18-20</sup>, this method targets the functional incorporated in the KS equation, which treats non-interacting kinetic energy explicitly, and thus burdens less with the machine-learning. Thanks to these advantages of the present strategy, the NN-based functional can learn the electron's characters efficiently even with a few systems, which significantly reduces the prerequisite cost of preparing the training dataset.

The training dataset were prepared by accurate electronic structure calculations<sup>21,22</sup> for three small molecules  $\text{H}_2\text{O}$ ,  $\text{NH}_3$ , and  $\text{NO}$  in their optimum atomic configurations. Note that this choice includes a spin-polarized system ( $\text{NO}$ ), which is necessary to determine the dependency on the spin polarization  $\zeta$ . The training was performed by Metropolis-type update of the weight parameters in the NN to minimize the error function regarding the atomization energies and density distributions: difference between those in the training dataset and those obtained by solving the KS equation with the NN-based functional.

Using the optimized NN functionals, we calculated properties of the hundreds of systems<sup>22,23</sup>, most of which are not included in the training dataset (Table 1). The performances are compared with the existing analytical LSDA<sup>8,9</sup>, GGA<sup>10-12</sup>, meta-GGA<sup>13-15</sup>, and hybrid<sup>24-26</sup> functionals. For all of the properties, even for unreferenced ones (the barrier heights and total energies), the NN-based functionals show better or comparable accu-

racies to the existing functionals in the respective levels. Remarkably, for the atomization energies, the NN-based NRA type functional shows the comparable accuracy to the hybrid functionals, which are fitted to far more reference dataset(100~). The NN-based functionals seems to have successfully extracted, from the small training dataset, electron's common characters which are crucial to accuracies for many other systems. Because of this NN's capability of capturing common characters, accuracies for unreferenced systems are expected to improve more by adding further available data of related systems. Also, by adding variables in functionals, the energy-related accuracies are systematically improved as well as accuracies for density distributions, as exhibited in Fig. 1. This result shows that systematic improvement of the functional is realized by adding further variables to  $\mathbf{g}$  and training with density distributions as recently suggested by Medvedev et al<sup>5</sup>.

We also applied the trained NN-based meta-GGA functional to  $\text{C}_2\text{H}_2$  and  $\text{N}_2$ , comparing to the existing meta-GGA functionals as shown in Fig.2. The smooth curves are not guaranteed in usual machine-learning methods skipping solving the KS equation, such as directly learning the energy-related quantities as a functional of atomic configurations<sup>18-20</sup>. This signifies the advantage of explicit solution of the KS equation, where the kinetic energy operator mitigates unphysical noises in the electron density due to the possible overfitting, leading to the transferability of the functional out of the training dataset, as shown in ref. 8.

The NN-based meta-GGA functional are analyzed by plotting enhancement factor from the xc-functional of LSDA<sup>8,9</sup>,

$$F_{xc}[n] \equiv \frac{\varepsilon_{xc}[n]}{\varepsilon_{xc}^{\text{LSDA}}(n, \zeta)} \quad (5)$$

which corresponds to energy density at the uniform electron gas(UEG) limit. As shown in Fig. 3, the NN-based functional behaves similarly in some parts to the analytical functionals. Especially, at the UEG limit (upper left panel), our functional shows close behavior to LSDA, even though there is no constraint to converge to the LSDA at the limit. Constructing xc-functional with the machine-learning approach can thus bypass the steps where human intuition is involved, such as introducing theoretically available approximations, representing the functional form in an analytically tractable form, or constraining asymptotic behaviors at some limits.

In summary, we propose the machine-learning approach to systematic development of the xc-functional in the KS DFT. Note that the NN-based functionals are constructed with minimal assumption on the functional form, unlike the existing functionals referring to several theoretical constraints which are available for human beings. Our results suggest that a systematic improvement can be further conducted with a rather simple procedure: Prepare a maximally flexible NN-based functional form and train it with some physical/chemical quanti-

ties and electron density distributions in some systems. These procedure yields comparable or even better functionals compared to the existing functionals constructed with the physical consideration, along which additional variables, such as  $R$ , are incorporated with less human effort. Unlike the improvement by introducing orbital-dependent terms<sup>4</sup>, our method keeps the classical framework of solving the KS equation with the ordinary DFT computational cost, which enables us widely transferable calculations. The present success exemplifies a novel path toward the numerically exact functionals alternative to the Jacob's ladder.

## DATA AVAILABILITY

The weights of the optimized NN parameters for the LSDA, GGA, meta-GGA and NRA cases are available in <https://github.com/ml-electron-project/NNfunctional>.

## ACKNOWLEDGEMENTS

R.N. thanks Takahito Nakajima and Yoshiyuki Yamamoto for comments at the initial stage of this study. Part of the calculations were performed at the Supercomputer Center at the Institute for Solid State Physics in the University of Tokyo.

## METHODS

### A. Structure of NN-based functional.

We formulate the xc-energy density as

$$\varepsilon_{xc}(n, \mathbf{g}) = -n^{\frac{1}{3}} \frac{1}{2} \left\{ (1 + \zeta)^{\frac{4}{3}} + (1 - \zeta)^{\frac{4}{3}} \right\} G_{xc}^{NN}(\mathbf{g}). \quad (6)$$

The first factor  $n^{\frac{1}{3}}$  corresponds to the Slater exchange energy density<sup>8</sup>, and the second one is from spin-scaling approximation for exchange energy of uniformly-spin-polarized electron gas<sup>27</sup>. They are the minimal physical conditions introduced to initial state of the NN close to the goal. The remaining correction  $G_{xc}^{NN}$  is constructed using the NN defined in Eq.3 with four layers:

$$G_{xc}^{NN}(\mathbf{g}) = 1 + h_4(\dots(h_1(\log \mathbf{g}))) \quad (7)$$

Note that each element of  $\mathbf{g}$  is preprocessed as shown below if included:

$$\begin{aligned} n &\rightarrow \log n^{\frac{1}{3}} \\ \zeta &\rightarrow \log \left( \frac{1}{2} \left\{ (1 + \zeta)^{\frac{4}{3}} + (1 - \zeta)^{\frac{4}{3}} \right\} \right) \\ s &\rightarrow \log s \\ \tau &\rightarrow \log \left( \frac{\tau}{n^{\frac{5}{3}} \left\{ (1 + \zeta)^{\frac{5}{3}} + (1 - \zeta)^{\frac{5}{3}} \right\}} \right) \\ R &\rightarrow \log R \end{aligned} \quad (8)$$

These transformations are introduced to facilitate the optimization of NN by making  $\mathbf{g}$  dimensionless, suppressing the change in the magnitude, and regularizing so that the variance ranges of all elements become similar to one another. For the activation function  $f$ , we adopted the non-linear activation function named "Exponential Linear Unit"<sup>28</sup>, which is defined as  $f(x) = \max(0, x) + \min(0, e^x - 1)$ . The last layer  $h_H$  is designed to keep the value of  $\varepsilon_{xc}$  to non-positive. The dimensions of the parameter matrices and bias vectors are as follows:  $\dim W_1 = N \times 100$ ,  $\dim W_2 = \dim W_3 = 100 \times 100$ ,  $\dim W_4 = 100 \times 1$ ,  $\dim b_1 = \dim b_2 = \dim b_3 = 100$ ,  $\dim b_4 = 1$ , where  $N$  represents the number of elements in  $\mathbf{g}$ .

### B. Functional with non-local density distribution.

We suggest a simple functional form treating non-locality:

$$E_{xc}[n] = \int d\mathbf{r} n(\mathbf{r}) \varepsilon_{xc}(\mathbf{g}[n](\mathbf{r})) \quad (9)$$

$$\mathbf{g}[n](\mathbf{r}) = (\mathbf{g}_{\text{local}}(\mathbf{r}), R(\mathbf{r})) \quad (10)$$

$$R(\mathbf{r}) = \int d\mathbf{r}' n(\mathbf{r}') d(\mathbf{r}, \mathbf{r}') \quad (11)$$

$\mathbf{g}_{\text{local}}(\mathbf{r})$  represents (semi-)local variables such as  $n(\mathbf{r})$ ,  $s(\mathbf{r})$ , or  $\tau(\mathbf{r})$ .  $d(\mathbf{r}, \mathbf{r}')$  is a weight function to include non-locality which vanishes at  $|\mathbf{r} - \mathbf{r}'| \rightarrow \infty$  limit. The functional derivative can be done as:

$$\begin{aligned} V_{xc}[n](\mathbf{r}) &= \frac{\delta E_{xc}}{\delta n(\mathbf{r})} \\ &= \frac{\partial e_{xc}(\mathbf{r})}{\partial \mathbf{g}_{\text{local}}(\mathbf{r})} \cdot \frac{\delta \mathbf{g}_{\text{local}}(\mathbf{r})}{\delta n(\mathbf{r})} + \int d\mathbf{r}' \frac{\partial e_{xc}(\mathbf{r}')}{\partial R(\mathbf{r}')} d(\mathbf{r}, \mathbf{r}') \end{aligned} \quad (12)$$

where  $e_{xc}(\mathbf{r})$  represents  $n(\mathbf{r}) \varepsilon_{xc}(\mathbf{g}[n](\mathbf{r}))$ .

We implemented those integration numerically on the same grid points to those used in the exchange-correlation integration. The cost of evaluating the xc-potential on all grids is proportional to the square of system size. In this work, we defined the  $\mathbf{g}$  as  $\exp(-|\mathbf{r} - \mathbf{r}'|/\sigma)$ .  $\sigma$  was fixed to 0.2 Bohr, which was derived from the inverse of the Fermi wavenumber in the H<sub>2</sub>O molecule estimated from the density distribution calculated by the CCSD calculation (averaged over the grids used for the numerical integration). The length is known to be the typical distance where the contribution to exchange-correlation hole at  $\mathbf{r}$  from  $\mathbf{r}'$  decays<sup>17</sup>.

### C. Training the NN-based functional.

We use the Monte Carlo method by repeating the following steps to train the NN:

1. At the  $t$ -th iteration, add a perturbation  $\delta\mathbf{w}^t$  to weights  $\mathbf{w}^t$  in NN.  $\mathbf{w}$  represents both elements in the matrices  $\{W_i\}$  and the vectors  $\{\mathbf{b}_i\}$ . Each element in  $\delta\mathbf{w}^t$  is generated randomly from normal distribution  $N(0, \delta w)$ .
2. Conduct the KS-DFT calculation for the target molecules and atoms to evaluate the cost function  $\Delta_{\text{err}}^i$  in Eq.14 using the NN-based functional with the weight-parameters  $\mathbf{w}^t + \delta\mathbf{w}^t$ .
3. According to a random number  $p$  generated from uniform distribution in (0,1) and the acceptance ratio  $P$  defined as below, decide whether to accept or reject the weight-perturbation  $\delta\mathbf{w}^t$ .

$$P = \exp\left(-\frac{\Delta_{\text{err}}^t - \Delta_{\text{err}}^{t-1}}{T}\right) \quad (13)$$

If  $P > 1$ : Set  $\mathbf{w}^{t+1} = \mathbf{w}^t$  and restart from step 1.

If  $p < P < 1$ : Set  $\mathbf{w}^{t+1} = \mathbf{w}^t + \delta\mathbf{w}$  and restart from step 1.

If  $P < p$ : Set  $\mathbf{w}^{t+1} = \mathbf{w}^t + \delta\mathbf{w}$  and restart from step 2.

We repeated those steps with making  $\delta w$  and  $T$  smaller, until the error function becomes small enough. The cost function  $\Delta_{\text{err}}$  is defined as:

$$\begin{aligned} \Delta_{\text{err}} = & c_1(\Delta^{\text{G2}}\text{AE}_{\text{H}_2\text{O}} + \Delta^{\text{G2}}\text{AE}_{\text{NH}_3} + \Delta^{\text{G2}}\text{AE}_{\text{NO}}) \\ & + c_2(\Delta^{\text{CCSD}}n_{\text{H}_2\text{O}} + \Delta n_{\text{NH}_3}^{\text{CCSD}} + \Delta^{\text{CCSD}}n_{\text{NO}}), \end{aligned} \quad (14)$$

$\Delta^{\text{G2}}\text{AE}$  represents the absolute deviation of the atomization energy in hartree from the G2 calculation. The  $\Delta^{\text{CCSD}}n$  represents the error between  $n$  obtained by the DFT and the CCSD calculation:

$$\Delta^{\text{CCSD}}n_M = \frac{1}{N_e} \sqrt{\int d\mathbf{r} (n_M^{\text{DFT}}(\mathbf{r}) - n_M^{\text{CCSD}}(\mathbf{r}))^2} \quad (15)$$

where  $N_e$  represents the number of electrons in the molecule  $M$ . The integrations are conducted numerically on grid points which is the same to those used in exchange-correlation integration of KS equation (See PySCF<sup>29</sup> document for details, the default DFT setting is adopted in all calculation through this work.).  $c_2/c_1$  was fixed to 10 hartree through the training.

In the training of each NN-based functional, the whole steps were conducted for about 300 times. The initial  $T$  and  $\delta W$  are set to 0.1 and 0.001. At the final step, they are reduced to 0.06 and 0.0005 respectively. The whole steps were conducted in parallel with 160 threads by ISSP System C, and the weight parameters which minimize the cost function the most were adopted finally.

#### D. Calculation conditions.

All of the DFT and the CCSD calculation in our work were implemented using PySCF<sup>29</sup> code with 6-311++G(3df,3pd) basis set was used for both in training

of NN-based functionals and in testing accuracies of the functionals. For the NN implementation, we used Pytorch package<sup>30</sup>.

TABLE I:

|            | AE147 <sup>a</sup><br>(kcal/mol) | DD147 <sup>b</sup><br>- | BH76 <sup>c</sup><br>(kcal/mol) | TE147 <sup>d</sup><br>(hartree) |
|------------|----------------------------------|-------------------------|---------------------------------|---------------------------------|
| SVWN       | 84.2                             | 0.0059                  | 15.4                            | 1.28                            |
| NN-LSDA    | 30.9                             | 0.0036                  | 13.8                            | 0.90                            |
| BLYP       | 7.3                              | 0.0024                  | 7.9                             | 0.41                            |
| PBE        | 17.0                             | 0.0018                  | 11.5                            | 0.21                            |
| NN-GGA     | 11.0                             | 0.0018                  | 9.6                             | 0.42                            |
| TPSS       | 6.2                              | 0.0017                  | 8.7                             | 0.48                            |
| SCAN       | 6.1                              | 0.0016                  | 7.7                             | 0.28                            |
| M06-L      | 5.2                              | 0.0019                  | 4.1                             | 0.42                            |
| NN-metaGGA | 4.7                              | 0.0013                  | 4.7                             | 0.14                            |
| PBE0       | 5.3                              | 0.0014                  | 5.0                             | 0.23                            |
| B3LYP      | 4.5                              | 0.0019                  | 4.7                             | 0.36                            |
| M06        | 3.7                              | 0.0019                  | 2.7                             | 0.35                            |
| NN-NRA     | 3.7                              | 0.0013                  | 5.5                             | 0.08                            |

**Table 1: Accuracies of NN-based functionals and other existing analytic functionals.** The values show mean absolute errors (MAE) for (a)the atomization energies (AE) of 147 molecules, (b)density distribution (DD, see Eq.15 in Method for the definition of the errors) evaluated from the CCSD<sup>21</sup> calculation for 147 molecules, (c)the chemical barrier heights of 76 reactions, and (d)total energies (TE) of 147 molecules from the G2 calculation<sup>22</sup>. The reference data for (a), (b), and (d) is cited from Ref. 22, and (c) is from ref. 23. The functionals with the prefix "NN" represents the NN-based functional with parameters trained through this work. All of the DFT and CCSD calculation are computed on 6-311++G(3df,3pd) basis set and implemented using PySCF<sup>29</sup>, except for the DFT calculation with existing LSDA, GGA, meta-GGA functionals for (c), which is cited from Ref.15, because some of those functionals implemented in PySCF show ill-convergence for the systems including H2. For the same reason, the H2 molecule in Ref.23 is excluded from the averages in (a), (c), and (d).

- 
- \* nagai-ryo236@g.ecc.u-tokyo.ac.jp
- <sup>1</sup> P. Hohenberg and W. Kohn, *Phys. Rev.* **136**, B864 (1964).
  - <sup>2</sup> W. Kohn and L. J. Sham, *Phys. Rev.* **140**, A1133 (1965).
  - <sup>3</sup> D. E. Rumelhart, G. E. Hinton, and R. J. Williams, *Nature* **323**, 533 EP (1986).
  - <sup>4</sup> J. P. Perdew and K. Schmidt, *AIP Conference Proceedings* **577**, 1 (2001).
  - <sup>5</sup> M. G. Medvedev, I. S. Bushmarinov, J. Sun, J. P. Perdew, and K. A. Lyssenko, *Science* **355**, 49 (2017).
  - <sup>6</sup> G. D. Mahan, *Many-Particle Physics* (Springer, 2000).
  - <sup>7</sup> R. Nagai, R. Akashi, S. Sasaki, and S. Tsuneyuki, *The Journal of Chemical Physics* **148**, 241737 (2018).
  - <sup>8</sup> J. C. Slater, *Phys. Rev.* **81**, 385 (1951).
  - <sup>9</sup> S. H. Vosko, L. Wilk, and M. Nusair, *Canadian Journal of Physics* **58**, 1200 (1980).
  - <sup>10</sup> A. D. Becke, *Phys. Rev. A* **38**, 3098 (1988).
  - <sup>11</sup> C. Lee, W. Yang, and R. G. Parr, *Phys. Rev. B* **37**, 785 (1988).
  - <sup>12</sup> J. P. Perdew, K. Burke, and M. Ernzerhof, *Phys. Rev. Lett.* **77**, 3865 (1996).
  - <sup>13</sup> J. Tao, J. P. Perdew, V. N. Staroverov, and G. E. Scuseria, *Phys. Rev. Lett.* **91**, 146401 (2003).
  - <sup>14</sup> J. Sun, A. Ruzsinszky, and J. P. Perdew, *Phys. Rev. Lett.* **115**, 036402 (2015).
  - <sup>15</sup> Y. Zhao and D. G. Truhlar, *The Journal of Chemical Physics* **125**, 194101 (2006).
  - <sup>16</sup> K. Hornik, *Neural Networks* **4**, 251 (1991).
  - <sup>17</sup> O. Gunnarsson, M. Jonson, and B. I. Lundqvist, *Phys. Rev. B* **20**, 3136 (1979).
  - <sup>18</sup> F. Brockherde, L. Vogt, L. Li, M. E. Tuckerman, K. Burke, and K.-R. Müller, *Nat. Commun.* **8**, 872 (2017).
  - <sup>19</sup> T. Xie and J. C. Grossman, *Phys. Rev. Lett.* **120**, 145301 (2018).
  - <sup>20</sup> A. Chandrasekaran, D. Kamal, R. Batra, C. Kim, L. Chen, and R. Ramprasad, *npj Computational Materials* **5**, 22 (2019).
  - <sup>21</sup> G. D. Purvis and R. J. Bartlett, *The Journal of Chemical Physics* **76**, 1910 (1982).
  - <sup>22</sup> L. A. Curtiss, K. Raghavachari, P. C. Redfern, and J. A. Pople, *The Journal of Chemical Physics* **106**, 1063 (1997).
  - <sup>23</sup> Y. Zhao, N. González-García, and D. G. Truhlar, *The Journal of Physical Chemistry A* **109**, 2012 (2005).
  - <sup>24</sup> M. Ernzerhof and G. E. Scuseria, *The Journal of Chemical Physics* **110**, 5029 (1999).
  - <sup>25</sup> P. J. Stephens, F. J. Devlin, C. F. Chabalowski, and M. J. Frisch, *The Journal of Physical Chemistry* **98**, 11623 (1994).
  - <sup>26</sup> Y. Zhao and D. G. Truhlar, *Theoretical Chemistry Accounts* **120**, 215 (2008).
  - <sup>27</sup> G. L. Oliver and J. P. Perdew, *Phys. Rev. A* **20**, 397 (1979).
  - <sup>28</sup> D.-A. Clevert, T. Unterthiner, and S. Hochreiter, *Under Review of ICLR2016* (2015).
  - <sup>29</sup> Q. Sun, T. C. Berkelbach, N. S. Blunt, G. H. Booth, S. Guo, Z. Li, J. Liu, J. D. McClain, E. R. Sayfutyarova, S. Sharma, S. Wouters, and G. K. Chan, *Wiley Interdisciplinary Reviews: Computational Molecular Science* **8**, 1217 (2018).
  - <sup>30</sup> A. Paszke, S. Gross, S. Chintala, G. Chanan, E. Yang, Z. DeVito, Z. Lin, A. Desmaison, L. Antiga, and A. Lerer, in *NIPS-W* (2017).



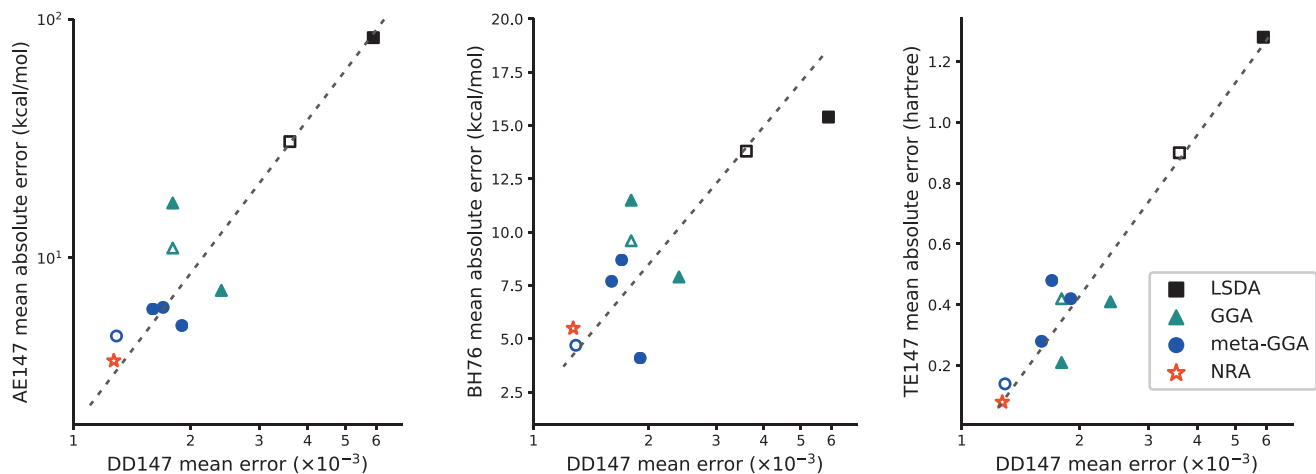


FIG. 1: Improving accuracies for the atomization energies (AE147), the reaction barrier heights (BH147), and the total energies (TE147) with improving accuracies for density distribution (DD147) and increasing variables in the functionals, corresponding to Table 1. The closed and open markers represent accuracies of existing and NN-based functionals respectively.

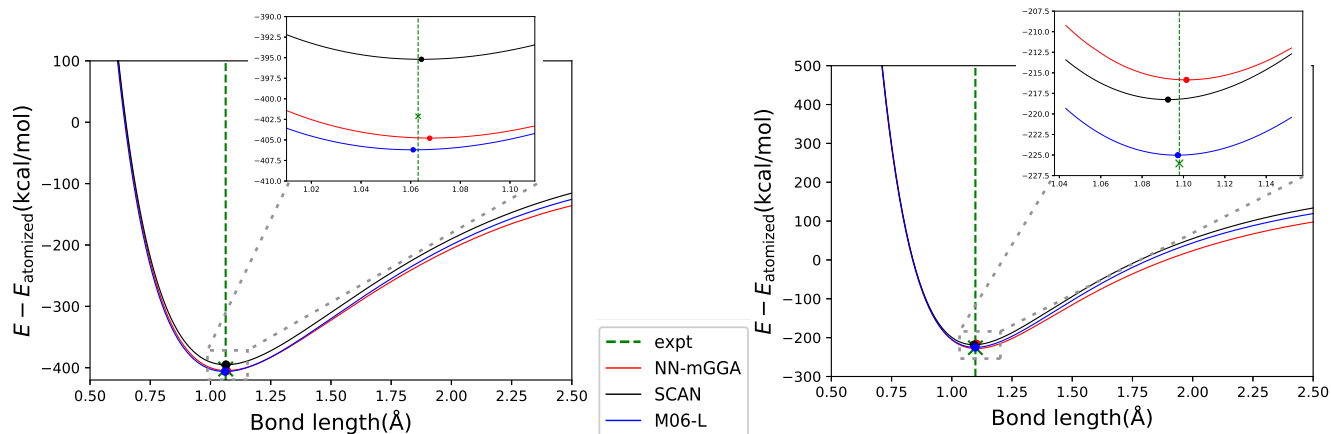


FIG. 2: Dissociation curve of the C-H bonds in C<sub>2</sub>H<sub>2</sub> (left) and the N-N bond in N<sub>2</sub> (right), calculated by the NN-based and existing meta-GGA functionals. Horizontal axis shows the bond length, and vertical axis shows relative energy from the atomized limit ( $E_{\text{atomized}}$ ). The green dashed lines and "x" marks show the bond lengths and the atomization energies from experiments<sup>22</sup>. The "o" mark shows the peak of each curve.

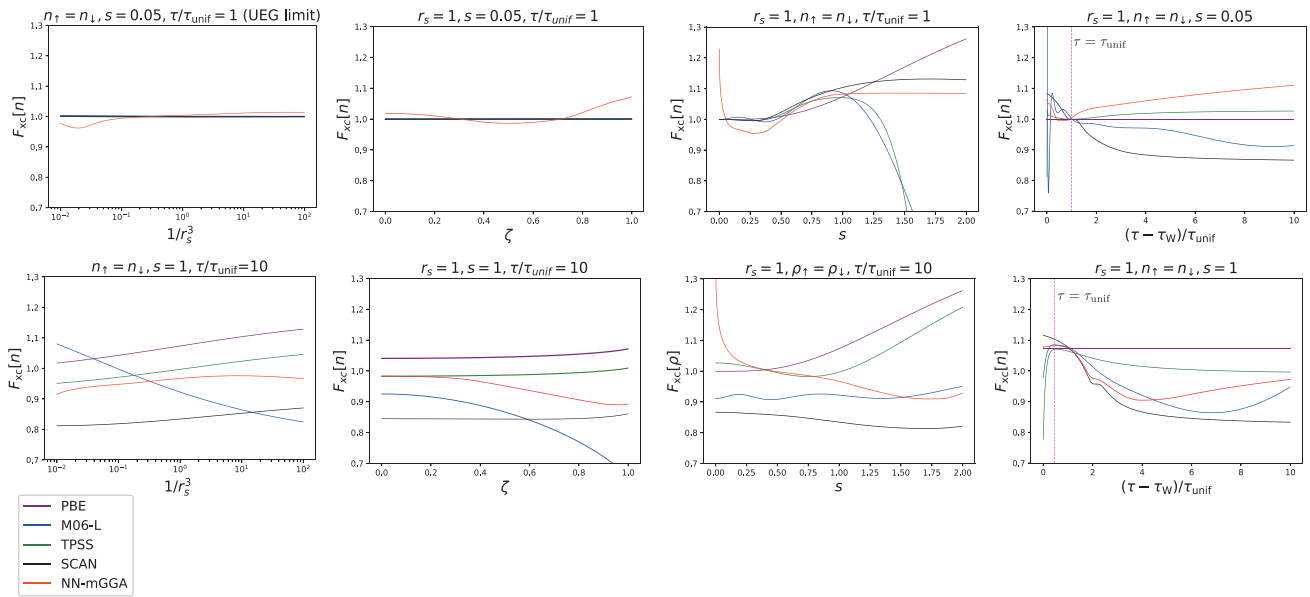


FIG. 3: Behaviors of functionals around typical ranges of density distributions. The vertical axis are defined as eq.. Meta-GGA type functionals have four variables, and the panels show the dependence on one of them while the others are fixed.  $r_s \equiv (3/4\pi n)^{1/3}$  represents average distance between electrons.  $\tau_{unif} \equiv (3/10)(3\pi^2)^{2/3}n^{5/3}$ ,  $\tau_W \equiv |\nabla n|^2/8n$  represents  $\tau$  at UEG limit and single-orbital limit respectively<sup>13</sup>.